Bathymetry Determination From Marine Radar Image Sequences Using the Hilbert Transform

Li-Chung Wu, Dong-Jiing Doong, and Jong-Hao Wang

***Abstract*— This letter presents an image processing technique based on the theory of the Hilbert transform to determine the coastal bathymetry from marine radar image sequences. Use of the Hilbert transform enables the difficulties and complications of inhomogeneous image analysis to be avoided. In addition, a number of steps and complex computations can be avoided using the numerical algorithm of the Hilbert transform. Because the Hilbert transform is suitable for only monocomponent signals, we first applied the image procedure to decompose the irregular wave patterns into different single wave period images. Analysis of the simulated wave field and radar image sequences demonstrated that there was a high correlation between the estimated depths and reference depths. The causes for errors in the bathymetry estimations are also discussed.**

***Index Terms*— Bathymetry determination, Hilbert transform, marine radar.**

I. Introduction

THE marine X-band radar, which is typically used to detect the coastline and obstacles on the sea surface, is currently one of the most widely used tools for ocean remote sensing. Different studies have confirmed the mechanism for imaging sea surface wind wave patterns using the X-band radar [1]. The feasibility of ocean wave and sea surface current observation was also demonstrated based on the principle of sea surface wave imaging [2], [3]. Following these studies, some studies proposed different algorithms to derive the bathymetry information from the gravity wave patterns on the X-band radar images. Bell [4] was the first to propose a complete procedure to determine the bathymetry from marine radar images. In this letter, the basic principle of the wave phase speed analysis was used to perform a cross-correlation analysis between subsequent images to track the motion of small areas in the wave pattern from the radar images. Subsequently, many studies proposed different methods to determine the bathymetry [5], [6]. Because the wave phase speed can be determined using the wave frequency and wavenumber, estimation of the local wavenumber is always important in determining the bathymetry in all of these studies. The wavenumber can be estimated from the image spectra, and the fast Fourier transform (FFT) is the most common algorithm used to obtain the image spectrum from the radar images. The assumption of spatial homogeneity within the analyzed area is necessary, regardless of which FFT or cross-correlation analysis method is implemented. However, it is generally acknowledged that the spatial wave signals from coastal radar images are highly nonhomogeneous. Some studies have proposed solutions to analyze the inhomogeneous wave images [5], [7]. However, a large number of steps and complex computations, such as 3-D FFT, filtering techniques, 2-D inverse FFT, and continuous Wavelet transform, are unavoidable. This letter attempted to estimate the local wavenumber using the Hilbert transform to determine the bathymetry using the marine radar images more rapidly. The Hilbert transform has been demonstrated to be a powerful tool to analyze frequency modulated signals. However, there is only one wavenumber value at any given spatial location of the image. Because the real wave images often have multiple components or are from a broadband spectrum, we must obtain monocomponent wave images prior to data analysis using the Hilbert transform. In the subsequent sections, we will demonstrate the entire image processing procedure and confirm its practicability using a simulated wave field and coastal radar images.

Manuscript received January 18, 2017; accepted February 7, 2017. Date of publication March 6, 2017; date of current version April 20, 2017.

L.-C. Wu is with the Coastal Ocean Monitoring Center, National Cheng Kung University, Tainan 70101, Taiwan.

D.-J. Doong is with the Department of Hydraulic and Ocean Engineering, National Cheng Kung University, Tainan 70101, Taiwan.

J.-H. Wang is with the Hydrology Division, Water Resources Agency Ministry of Economic Affairs, Taipei 10651, Taiwan

Color versions of one or more of the figures in this letter are available online at http://ieeexplore.ieee.org.

Digital Object Identifier 10.1109/LGRS.2017.2668383

II. Theoretical Preliminaries

Although some studies have proposed different methods to determine the bathymetry from coastal remotely sensed images, the theory of the wave dispersion relationship is still critical for all studies of bathymetry determination from wave field radar images. Assuming that the wave–current interaction is neglected, the bathymetric inversion equation can be described as [5]

$$d(x, y) = (L_0/2\pi)[C(x, y)/C_0] \tanh^{-1}(C/C_0) \tag{1}$$

where $d(x, y)$ and $C(x, y)$ are the water depth and wave phase speed at different locations (x, y) and L_0 and C_0 are the wavelength and wave phase speed in deep water, respectively. L_0 and C_0 can be estimated using the wave period T and acceleration due to gravity g

$$L_0 = gT^2/2\pi \tag{2}$$

$$C_0 = gT/2\pi. \tag{3}$$

As noted above, the Hilbert transform should fail to accurately estimate the local wavenumber from the wave image signals, which are multicomponents. We have to decompose the original wave image signals into different monocomponent signals. The image decomposition methods [4] were implemented in this letter. Based on linear wave theory, the wave period is independent of the bathymetry, and thus, the wave period is constant during wave propagation.

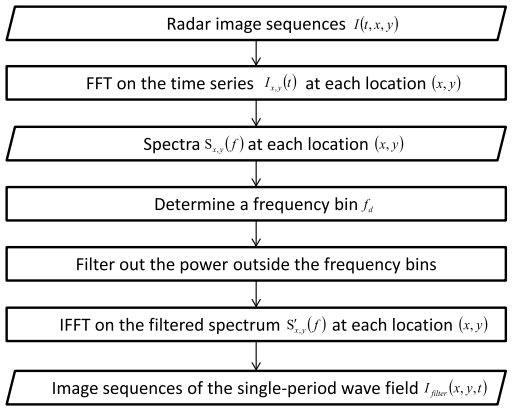

Fig. 1. Flowchart for obtaining the image sequences of single-period wave field.

As shown in Fig. 1, the time series $I_{x,y}(t)$ at each pixel (x, y) of the radar image sequences $I(t, x, y)$ is transformed into the frequency spectra $S_{x,y}(f)$ using 1-D FT. For the spatial image with $M \cdot N$ pixels, we can obtain $M \cdot N$ frequency spectra $S_{x,y}(f)$ after the FT. For each spectrum, the power density is distributed into different frequency bins. To obtain the monocomponent signals, we preserve the power density at only one specific frequency bin f_d

$$S'_{x,y}(f) = S_{x,y}(f) \cdot S_{\text{filter}}(f)$$

where

$$S_{\text{filter}}(f) = \begin{cases} 1 & f = f_d \\ 0 & f \neq f_d. \end{cases} \tag{4}$$

This spectral filtering is carried out on individual pixels in isolation. After filtering the spectra at all locations in the image, we can obtain the single-period wave field $I_{\text{filter}}(t, x, y)$ using the 1-D inverse FFT (IFFT) of the filtered spectra at each location. Based on the wave dispersion relationship, longer period (lower frequency) waves require the determination of deeper bathymetry. In addition, longer period waves are less influences of wave–current interaction on the dispersion relationship. To avoid the sea surface waves that are not sufficiently long to be used in correctly analyzing the bathymetry, we used the frequency bins f_d whose periods are greater than 7 s.

After the image processing outlined above, we can obtain T images of a single-period wave field from T original radar images. Although the period is invariant, these reconstituted wave signals on the image are wavenumber modulated due to the influence of bathymetry. Then, we can apply the Hilbert transform to estimate the local wavenumber from $I_{\text{filter}}(t, x, y)$.

The Hilbert transform provides a method to define the imaginary part of the signals, and we can estimate the signal phase and instantaneous frequency from the phase derivative. In this letter, this method was implemented to analyze the spatial image and estimate the wavenumber. Unlike the temporal data, there are two dimensions in the spatial domain. Hence, the series along the x- and y-directions inside the image are analyzed. The Hilbert transform is applied for each row (along *x-direction*) of the wave field image

$$H\{I_{\text{filter}}(x, y_m)\} = I_{\text{filter}}(x, y_m) * (1/\pi x) \tag{5}$$

where $*$ is the convolution operator and y_m indicates the mth row. Each row inside the image matrix is analyzed using (5). In the field of discrete signal processing, the Hilbert transform algorithm can be implemented more effectively using an FFT algorithm. Based on the theory of the Hilbert transform, the signal processing using this method can be treated as a phase shifter that shifts the phase of every sinusoidal function by $-90°$. Hence, the studies of Gabor can be implemented [8]. We can calculate the FT of the given signal and suppress the amplitudes belonging to negative frequencies. Then, we multiply the amplitudes of the positive frequencies by two. Finally, a complex-valued signal with real and imaginary parts that form a Hilbert-transform pair can be obtained from the IFFT of the filtered spectrum. The complex-valued signals, which contain $I_{\text{filter}}(x, y_m)$ as the real part and $H\{I_{\text{filter}}(x, y_m)\}$ as the imaginary part, are the analytic signals in the space domain. The local phase from each row of the wave field image can be obtained by computing the arctangent of the analytic signal as

$$\varphi_x(x, y_m) = \arctan[H\{I_{\text{filter}}(x, y_m)\}/I_{\text{filter}}(x, y_m)]. \tag{6}$$

After calculating the gradient of the local phase, we can obtain the local wavenumber

$$k_x(x, y_m) = \Delta\varphi_x(x, y_m)/\Delta x. \tag{7}$$

TABLE I
COMPUTATIONAL COMPLEXITIES OF LOCAL WAVENUMBER ESTIMATION

Algorithm	Computational complexity
DiSC method [5]	$O\big(T \cdot M \cdot N \cdot \log(T \cdot M \cdot N) + M \cdot N \cdot \log(M \cdot N)\big)$
Continuous wavelet transform [7]	$O\big(T \cdot M^2 \cdot N^2 \cdot \log(M \cdot N)\big)$
Hilbert transform	$O\big(2 \cdot T \cdot M \cdot N \cdot \log(M \cdot N)\big)$

Table I shows the computational complexities of local wavenumber estimation from the image sequences whose data length is $T \cdot M \cdot N$ using different methods. Because the core algorithms of the Hilbert transform are only based on the 2-D FFT and IFFT, the computational complexity is lower than other methods.

Equations (5)–(7) can be used again to analyze the local wavenumber along the y-direction of the wave field image. Then, we can obtain the local wavenumber in two dimensions, $\vec{k} = (k_x, k_y)$. The local wave phase speed from each location of the wave filed can be estimated using wave theory

$$C_i = (2\pi f_d)/|\vec{k}(x, y)|. \tag{8}$$

Once the local wave phase speed is estimated using (8), we can determine the bathymetry using (1). The entire flowchart is shown in Fig. 2.

TABLE II

PARAMETER SETTINGS OF THE SIMULATED IMAGE SEQUENCES. THE NUMBER OF GRID POINTS IS A POWER OF 2. THE SETTINGS OF TIME INTERVAL AND GRID SIZE FOLLOW THE FORMATS OF MARINE RADAR IMAGES

Parameter	Value
Number of grid points (t-direction; x-direction; y-direction)	128; 512; 512
Time interval of the image sequence ($\triangle t$)	1.43 sec
Grid size of the spatial image ($\triangle x$ and $\triangle y$)	7.5 m

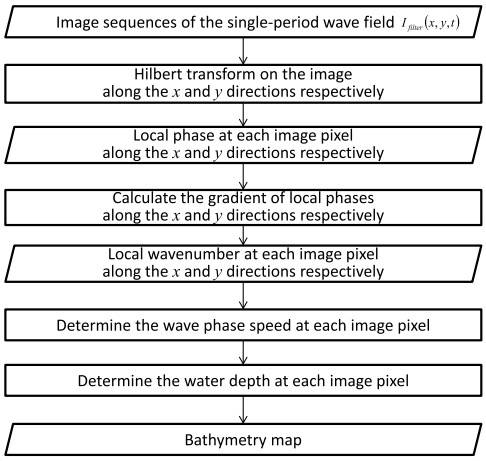

Fig. 2. Flowchart for determining the bathymetry map from a single-period wave field.

III. DATA ANALYSIS

Both the simulated sea surface image sequences and the coastal radar image sequences were used in this letter to verify the practicability of the bathymetry map determination using the Hilbert transform. For the simulated wave field, we used the linear superposition of different regular wave components, each having a dominant frequency and propagation direction. Considering the propagation of waves in shallow water, the irregular wave simulation was based on the TMA wave spectrum which is from the names of the data sets TEXEL, MARSEN, and ARSLOE. The TMA spectrum is intended for use in water of finite depth and is derived from the JONSWAP (JOint North Sea WAve Project) spectrum. The complete theory and procedure of irregular wave field signals is provided in [9]. In this letter, initial wave conditions of a 1.5 m significant wave height, a 315° dominant wave direction, and an 8 s mean wave period were used to simulate the image sequences of the wave field. The parameters of the simulated image sequences are provided in Table II. To implement the FFT algorithm, the numbers of grid points in the time domain (t-direction) and space domain (x- and y-directions) were powers of 2. The time interval and grid size of the simulated image sequences were the same as those of the marine radar image sequences, which we will analyze later. Considering the low grazing angle radar backscatter from the ocean surface, the effects of shadowing and tilt modulation are included in our simulated wave field image. The methods to simulate the wave field images with the effects of shadowing and tilt modulation are based on the study in [10]. For the scenario of radar observation, the distance between the radar antenna and the south edge of wave field image is 600 m. The height of radar antenna is 15 m from the mean sea level.

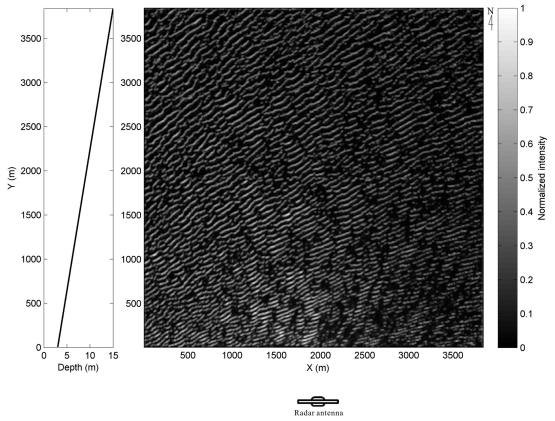

Fig. 3. Simulated irregular wave image and its corresponding bathymetry. Changes in wave direction and wavelength along the y-direction can be detected by changes in the bathymetry.

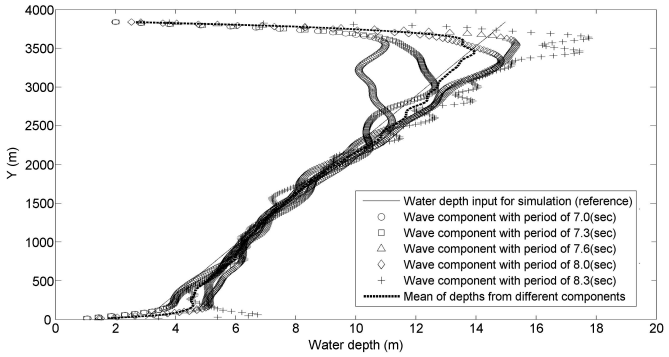

Fig. 4. Depth estimations using different single-period wave fields. The differences are particularly notable at the edges of the wave field due to Gibbs phenomena at the first and last data points.

The simulated irregular wave image is shown in Fig. 3. Due to the effects of shadowing and tilt modulation, the intensities at the facets that are close to the wave crests and face the radar antenna are much stronger than at other areas of the sea surface. For our simulation case, the water depth was invariant along the x-direction but decreased linearly from north to south. The wave refraction can be identified from the wave field image due to the influence of the bathymetry. Because this irregular wave field image was composed of different wave components, the simulated images were decomposed into different single-period wave fields before implementing the Hilbert transform. For each single wave period case, we can obtain 128 images with a size of 512 pixels × 512 pixels. This means that 128 local wavenumber values can be obtained from each location of the wave field using the Hilbert transform. The local wavenumber estimation using the Hilbert transform is sensitive to the wave profile of the images. Although the wave decomposition is implemented before the Hilbert transform, some unstable local wavenumbers are still unavoidable. To determine one reliable wavenumber value from one location of the image, the most frequent value from 128 estimated wavenumber values is used. After determining the applicable wavenumber values along the x- and y-directions, we can estimate the bathymetry from the different locations of the wave field using (1). Because of the less computational complexity

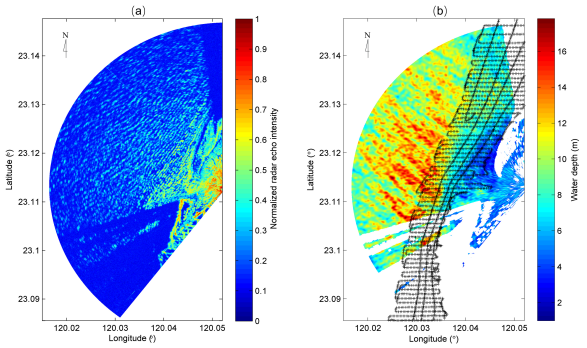

Fig. 5. (a) Radar image observed for the bathymetry determination. The wave pattern can be recognized in the northwestern part of the image. Due to the shadowing of the windbreak forest, the range of the azimuth that is observable for the wave patterns was approximately 110°. (b) Bathymetry results. (Cross symbols) Tracking of *in situ* measurements.

using the Hilbert transform which is shown in Table I, the local bathymetry of this case can be estimated within 5 min using a single personable computer.

Fig. 4 shows the results of the depth estimation from different single-period images. As discussed in the previous section, the frequency bins f_d with periods greater than 7 s were used to obtain the single-period images. Because the input water depth from our simulation is invariant along the x-direction, we focus on only the estimated bathymetry along the y-direction. Although the estimated depth values are similar to the input values, the differences between the simulated and estimated values of the water depth are still detectable. This result is likely due to the sensitivity of the Hilbert transform to waves with small-scale unstable wave profiles. Additionally, the differences are particularly notable at the edges of the wave field due to the end effects of the Hilbert transform. As noted above, the numerical method used to implement the Hilbert transformation is based on the FFT. The finite data length change contributes to oscillations of the local wavenumber due to Gibbs phenomena. As a result, the first and last points of the data are typically inaccurate after Hilbert transform. We average the depth values from five different wave components to reduce the oscillations in the depth estimation. As shown in Fig. 4, the mean depths were more consistent with the reference values. The Pearson product-moment correlation coefficient between the mean estimated depths and reference depths was 0.92. Fig. 4 also reveals the underestimation of water depths in deep water area using the wave components of shorter wave periods. We will discuss this issuelater.

After examining the validity of the technique presented in this letter, the marine radar image sequences were used to test the algorithm. The image cases in this letter were collected from a marine radar system installed on the western coast of Taiwan. The radar had a peak power output of 25 kW and operated at 9.4 GHz (X-band) with HH polarization. The 6.5-foot-long antenna had a horizontal beamwidth of 1.2° and a rotation rate of 42 rpm, yielding an image sequence sampling rate of 0.7 Hz. The antenna was installed at a height of 15 m. We collected images over a range within 3750 m with a grid size of 7.5 m($\triangle x = \triangle y = 7.5$ m). The system stores the

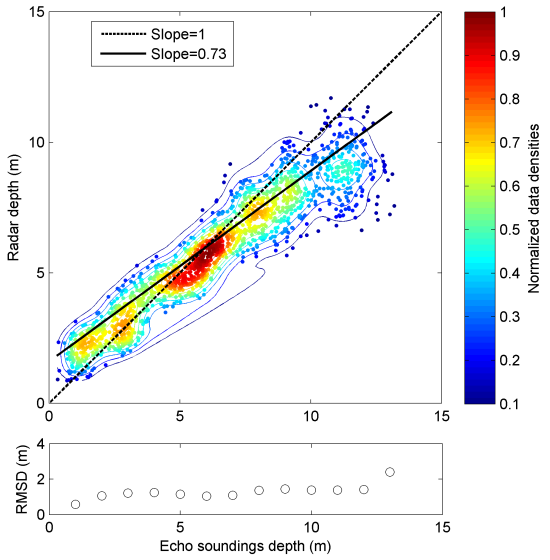

Fig. 6. Scatter plot of the water depth determined from the radar images and the *in situ* data from the echo sounder. The correlation coefficient between the two data sets was 0.94. The root-mean-square deviation between the estimated and reference depths is higher in deep water area.

logarithmically amplified radar backscatter information at a 12-b image depth. The significant wave height and mean wave period during our field experiment are 2.1 min and 5.0 s. Fig. 5(a) shows the radar images, which present the wave patterns in the northwest part of the image. The same five frequency bins f_d that were used to analyze the simulated wave images were also applied here to obtain the single-period wave images from the marine radar images. We averaged the depth values from five different wave components. The colors in Fig. 5(b) indicate the mean bathymetry results estimated from the radar images. For the method of Hilbert transform, the local wavenumber from each pixel of the radar image can be estimated. As a result, the best spatial resolution of bathymetry map equals the spatial resolution of radar images. The spatial moving average within the window of 5 pixels × 5 pixels is applied to reduce the uncertainty of estimated bathymetry map. The *in situ* depth values were used to verify the depth estimation from the radar images. The *in situ* bathymetry was measured using the single beam echo sounder. The influences of the tide and swell were corrected during the measurement. The radar observation for this case was performed four months after the echo sounder measurements. For comparison with the *in situ* data, we corrected for the tidal influences on the radar observation using the *in situ* water level measured from the neighboring tide station. Approximately 1600 *in situ* depth samples were measured within the radar observation area.

Fig. 6 compares the water depth retrieved from the radar images and the *in situ* data from the echo sounder. The correlation coefficient between the two data sets is 0.94. However, differences between the radar depths and echo sounding depths could still be observed. The possible reasons for the differences are summarized as follows.

1) *Asynchronous Data Sets*: The *in situ* measurements were performed four months earlier than the radar observation. During this time gap, the coastal bathymetry in

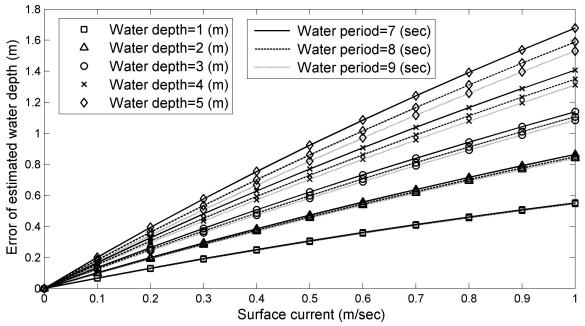

Fig. 7. Influence of surface current on estimating the water depth using wave dispersion relationship. The higher error of estimated water depth is observed if stronger surface current exists.

our study site may have changed due to the influence of sea states.

2) *Unclear Wave Patterns*: The wave pattern is important for estimating the local wavenumber. The estimation of the local wavenumber using the Hilbert transform could be inaccurate if the wave pattern is not sufficiently clear.
3) *Limitations of Linear Wave Theory*: Fig. 6 shows that the radar-derived depths are overestimated in shallow water area. Unlike the simulated wave field above, wave breaking and nonlinear effects of natural waves in the very shallow water area are unavoidable. The accuracies of derived depths based on linear wave theory should be limited in the very shallow water area. Although some studies have tried to implement the nonlinear wave theory [11], the linear wave dispersion relationship is still the most practical method for bathymetry estimations in most of the similar studies.
4) *Influence of Surface Current*: In addition to wave breaking and nonlinear effect, the accuracy of shallow water depth estimation is also influenced by surface current in case the current is strong. As mentioned above, the wave–current interaction is assumed to be neglected while using dispersion relationship. Fig. 7 shows that the error of estimated water depth can be obvious if the surface current is strong. Because the tidal current is often slack while high tide or low tide, the image cases observed at these events should be helpful. In addition, Fig. 7 also shows that image cases with longer period waves can reduce the effects of strong surface current.
5) *Wave Period is Not Long Enough*: The regression line and root-mean-square deviation in Fig. 6 show the underestimation of radar derived depths in deep water. In case the wave period is not long enough, the influence of water depth in deep water cannot be estimated accurately from the wave dispersion relationship.

IV. Conclusion

Coastal bathymetric information is necessary for different applications, such as planning shipping routes and coastal protection. Underwater acoustics techniques are the most useful ways to obtain high-precision depth data. However, the operation risk and cost of such *in situ* techniques must be considered.

Remote sensing using marine X-band radar may be a potential way to obtain coastal bathymetric information. Because the wave patterns on the radar images are important for extracting the water depth, different algorithms have been proposed to analyze the wave pattern images. This letter proposes a method based on the Hilbert transform theory to address nonhomogeneous wave patterns. A large number of steps and complicated computations can be avoided because the local wavenumber can be determined easily using the Hilbert transform. We can obtain the bathymetric results for each image sequence analysis case within 10 min using a common personal computer.

The simulated wave field and coastal radar image sequences were used to verify the practicability of the bathymetry determination using the Hilbert transform. A comparison between the estimated depth values and the reference values indicated high correlations. However, the differences between the estimation and the reference depths are still detectable. Errors can arise in the bathymetry estimation for several reasons. For the Hilbert transform algorithm, errors are unavoidable at the edges of the wave field due to the effects of Gibbs phenomena. In addition, linear wave theory, which is used to determine the bathymetry, will be limited in the shallower water areas. With respect to the conditions of the ocean waves, the wave patterns must be sufficiently clear to estimate the local wavenumber. The study and discussion of these cases demonstrated that bathymetry determination using marine radar image sequences and the Hilbert transform is feasible.

References

[1] M. G. Mattie and D. Lee Harris, "The use of imaging radar in studying ocean waves," in *Proc. 16th Conf. Coast. Eng.*, Hamburg, Germany, 1978, pp. 174–189.
[2] I. R. Young, W. Rosenthal, and F. Ziemer, "A three-dimensional analysis of marine radar images for the determination of ocean wave directionality and surface currents," *J. Geophys. Res. Oceans*, vol. 90, no. C1, pp. 1049–1059, 1985.
[3] J. C. N. Borge, K. Reichert, and J. Dittmer, "Use of nautical radar as a wave monitoring instrument," *Coast. Eng.*, vol. 37, nos. 3–4, pp. 331–342, 1999.
[4] P. S. Bell, "Shallow water bathymetry derived from an analysis of X-band marine radar images of waves," *Coast. Eng.*, vol. 37, nos. 3–4, pp. 513–527, 1999.
[5] C. M. Senet, J. Seemann, S. Flampouris, and F. Ziemer, "Determination of bathymetric and current maps by the method DiSC based on the analysis of nautical X-band radar image sequences of the sea surface (November 2007)," *IEEE Trans. Geosci. Remote Sens.*, vol. 46, no. 8, pp. 2267–2279, Aug. 2008.
[6] F. Serafino, C. Lugni, J. C. N. Borge, V. Zamparelli, and F. Soldovieri, "Bathymetry determination via X-band radar data: A new strategy and numerical results," *Sensors*, vol. 10, no. 7, pp. 6522–6534, 2010.
[7] L.-C. Wu, L. Z.-H. Chuang, D.-J. Doong, and C. C. Kao, "Ocean remotely sensed image analysis using two-dimensional continuous wavelet transforms," *Int. J. Remote Sens.*, vol. 32, no. 23, pp. 8779–8798, 2011.
[8] D. Gabor, "Theory of communication. Part 1: The analysis of information," *J. Inst. Elect. Eng.*, vol. 93, no. 26, pp. 429–441, Jul. 1946.
[9] L. Z.-H. Chuang and L.-C. Wu, "Study of wave group velocity estimation from inhomogeneous sea-surface image sequences by spatiotemporal continuous wavelet transform," *IEEE J. Ocean. Eng.*, vol. 39, no. 3, pp. 444–457, Jul. 2014.
[10] S. Salcedo-Sanz, J. C. N. Borge, L. Carro-Calvo, L. Cuadra, K. Hessner, and E. Alexandre, "Significant wave height estimation using SVR algorithms and shadowing information from simulated and real measured X-band radar images of the sea surface," *Ocean Eng.*, vol. 101, pp. 244–253, Jun. 2015.
[11] S. Flampouris, J. Seemann, C. Senet, and F. Ziemer, "The influence of the inverted sea wave theories on the derivation of coastal bathymetry," *IEEE Geosci. Remote Sens. Lett.*, vol. 8, no. 3, pp. 436–440, May 2011.